Quantum Electronics **51** (6) 464–472 (2021)

https://doi.org/10.1070/QEL17583

Implementation of one-qubit quantum gates with individual addressing of two rubidium atoms in two optical dipole traps

I.I. Beterov, E.A. Yakshina, D.B. Tretyakov, V.M. Entin,
N.V. Al'yanova, K.Yu. Mityanin, A.M. Faruk, I.I. Ryabtsev

Abstract. **We report the results of experiments on implementing individually addressable one-qubit quantum gates on a microwave transition with two ^{87}Rb atoms in two optical dipole traps. Addressing is carried out using additional focused laser light, which results in a differential light shift of the microwave transition frequency. In the absence of addressing in each of the atoms, Rabi oscillations are obtained on the microwave clock transition $5S_{1/2}$ ($F = 2$, $m_F = 0$) → $5S_{1/2}$($F = 1$, $m_F = 0$) between two working levels of qubits with a frequency of up to 5.1 kHz, a contrast up to 98%, and a coherence time up to 4 ms. When addressing is turned on, the probability of a microwave transition in the addressed atom is suppressed to an average value of less than 5%. The Rabi oscillations remaining in the other atom have the same contrast and correspond to the implementation of individually addressable basic one-qubit quantum operations (Hadamard gate and NOT gate) from different initial states of a qubit with an average fidelity of 92% ± 3%. After renormalising this fidelity to the error in the preparation and measurement of quantum states of qubits, an estimate of 97% ± 3% is obtained for the fidelity of individual qubit rotations.**

Keywords: *single atoms, optical traps, one-qubit gates.*

1. Introduction

Experimental implementation of a quantum computer with qubits based on single neutral atoms in arrays of optical dipole traps requires addressing of individual qubits to perform basic one- and two-qubit quantum gates [1–5]. In the general case, the addressing in an array of traps is performed using focused laser light; in this case, the diameter of its waist should be smaller than the separation between neighbouring atoms in the array.

I.I. Beterov Rzhanov Institute of Semiconductor Physics, Siberian Branch, Russian Academy of Sciences, prosp. Akad. Lavrent'eva 13, 630090 Novosibirsk, Russia; Novosibirsk State University, ul. Pirogova 2, 630090 Novosibirsk, Russia; Novosibirsk State Technical University, prosp. K. Marksa 20, 630092 Novosibirsk, Russia;
E.A. Yakshina, D.B. Tretyakov, V.M. Entin, N.V. Al'yanova, K.Yu. Mityanin, I.I. Ryabtsev Rzhanov Institute of Semiconductor Physics, Siberian Branch, Russian Academy of Sciences, prosp. Akad. Lavrent'eva 13, 630090 Novosibirsk, Russia; Novosibirsk State University, ul. Pirogova 2, 630090 Novosibirsk, Russia; e-mail: ryabtsev@isp.nsc.ru;
A.M. Faruk Novosibirsk State University, ul. Pirogova 2, 630090 Novosibirsk, Russia; Department of Mathematics, Faculty of Science, Al-Azhar University, Nasr City 11884, Cairo, Egypt

Received 17 March 2021
Kvantovaya Elektronika **51** (6) 464–472 (2021)
Translated by V.L. Derbov

In the first experimental works demonstrating individual addressing with Rb atoms, one-qubit quantum gates were performed based on Raman transitions between two hyperfine sublevels of the ground state, which are the working levels of qubits [6, 7]. Raman transitions were induced by two-frequency laser light focused on a single atom in one of the traps. However, it was not possible to achieve high fidelity in performing one-qubit gates with this method because of rather large phase noise of laser light, which limits the coherence time to tens of microseconds or less with an instability of the frequency difference of Raman lasers of several kilohertz.

Much longer coherence times are provided by microwave clock transitions in alkali metal atoms (6.837 GHz for ^{87}Rb atoms, 9.193 GHz for ^{133}Cs atoms). To excite them, highly stable microwave generators with digital frequency synthesisers are used, having a linewidth of less than 100 Hz and a coherence time of up to tens of milliseconds. However, the wavelength of such radiation (several centimetres) significantly exceeds the size of atomic arrays (less than 100 μm), and so it affects all atoms simultaneously. For individual addressing at microwave transitions, the use of nonresonant laser radiation focused on one of the atoms was first proposed and implemented in [8]. Due to the large frequency detuning, it does not induce optical transitions between atomic levels, but causes a light shift of the qubit levels due to the dynamic Stark effect. Since the two working levels of a qubit undergo slightly different light shifts, the microwave transition frequency in the addressing laser field is shifted relative to the transition frequency in a free atom. If the frequency of the microwave generator is detuned by a certain amount from the exact frequency, then the addressing laser field can adjust it to exact resonance with the microwave field. Alternatively, the frequency of the microwave generator can be tuned to an exact resonance, and the addressing laser field can bring it out of resonance for the addressed qubits.

At present, this method of individual addressing provides the highest fidelity in performing one-qubit quantum gates. In recent papers [9, 10], the error in performing one-qubit quantum gates was demonstrated to be less than 0.01% for global addressing of all qubits and less than 0.2% for addressing of individual qubits.

In our recent studies, experiments were carried out both on the trapping of a single Rb atom in a single optical dipole trap [11] and ensembles of Rb atoms in trap arrays [12], and on the implementation of a one-qubit quantum gate on a microwave transition in a single Rb atom in a single trap [13]. A specific feature of the experiments performed is the formation of traps using a long-focus objective lens with a small numerical aperture (NA = 0.172) and a large focal length (f = 119 mm), located outside the vacuum chamber of a magneto-

optical trap (MOT). Long-focus objectives with a small numerical aperture are commonly used in the implementation of optical dipole traps for trapping large ensembles of atoms [14–18]. However, for traps with single atoms, such a scheme can potentially provide a higher fidelity in performing two-qubit quantum gates based on short-term laser excitation of atoms to Rydberg states [1–3]. In our scheme, atoms are far from all surfaces, on which working atoms are gradually deposited, which leads to the formation of parasitic charges and electric fields that strongly affect Rydberg atoms. Another feature is the use of a relatively cheap digital sCMOS video camera for recording single atoms by the resonance fluorescence signal instead of the commonly used expensive EMCCD cameras.

The goals of this work were the implementation of two optical dipole traps loaded with single Rb atoms and the demonstration of basic one-qubit quantum operations (Hadamard gate and NOT gate) based on individually addressable microwave transitions in an existing experimental setup with a long-focus lens and an sCMOS video camera.

2. Experimental setup

The basic optical diagram of the experimental setup is shown in Fig. 1. Initially, Rb atoms are cooled and trapped in a MOT in a vacuum chamber, in the centre of which a cloud of cold atoms with a temperature of 80–100 μK is formed. Then, to trap atoms from the MOT into an optical dipole trap, use is made of the radiation of a laser system with a wavelength of 850 nm, based on an Eagleyard EYPDFB-0852 master laser with distributed feedback and a Toptica Boosta Pro semiconductor amplifier with an output power of 1.4 W. The radiation power can be modulated using an acousto-optic modulator (AOM). This radiation is mixed with a 780 nm 'ejecting' laser radiation by means of a glass beam splitter BS. It is necessary to determine the quantum states of two atoms after performing one-qubit gates [13]. Further, the radiation is fed into the optical system through an optical fibre, which serves as a spatial filter.

After leaving the optical fibre, the radiation of the dipole trap laser and the ejecting one is collimated and reflected from the spatial light modulator, which forms a phase mask and transforms the wavefront of both beams forming a set of intensity maxima corresponding to two or more dipole traps at the lens focus [5, 12, 19]. Setting the wavefront also allows the distance between the traps to be controlled. Then the radiation of both lasers is passed through a polarisation beam splitter PBS, where the radiation of the addressing laser with a wavelength of 795 nm is added to them. It is necessary for individual addressing of microwave radiation to one of the traps due to the differential light shift of the microwave transition frequency. The addressing beam is moved using an acousto-optic deflector (AOD).

Then the radiation of the three lasers arrives at the dichroic mirror. It has a reflectivity of more than 95% at a wavelength of 850 nm, and about 7% at a wavelength of 780 nm (for radiation with a wavelength of 780 nm, a power of less than 1 mW is required). The radiation reflected from the dichroic mirror is focused into a cloud of cold Rb atoms by an objective lens with a focal length f = 119 mm and a numerical aperture NA = 0.172. This objective was designed and used for the first time in Ref. [20]. An expanding telescope consisting of two lenses with focal lengths increased in comparison with our previous works [11–13] (f = 75 mm and 450 mm instead of f = 25 mm and 150 mm) is installed in front of the objective. This reduced the aberrations in the optical system and made it possible to obtain waists with a diameter of 8–9 μm (measured at the intensity level e^{-2}) instead of 10–11 μm. This diameter should provide loading of predominantly single atoms due to the effect of light-induced collisional blockade [21].

To visualise the image of two trapped Rb atoms, resonant fluorescence induced by cooling laser radiation with a wavelength of 780 nm (not shown in Fig. 1) is used. The spontaneously emitted photons are collected by the same lens with f =

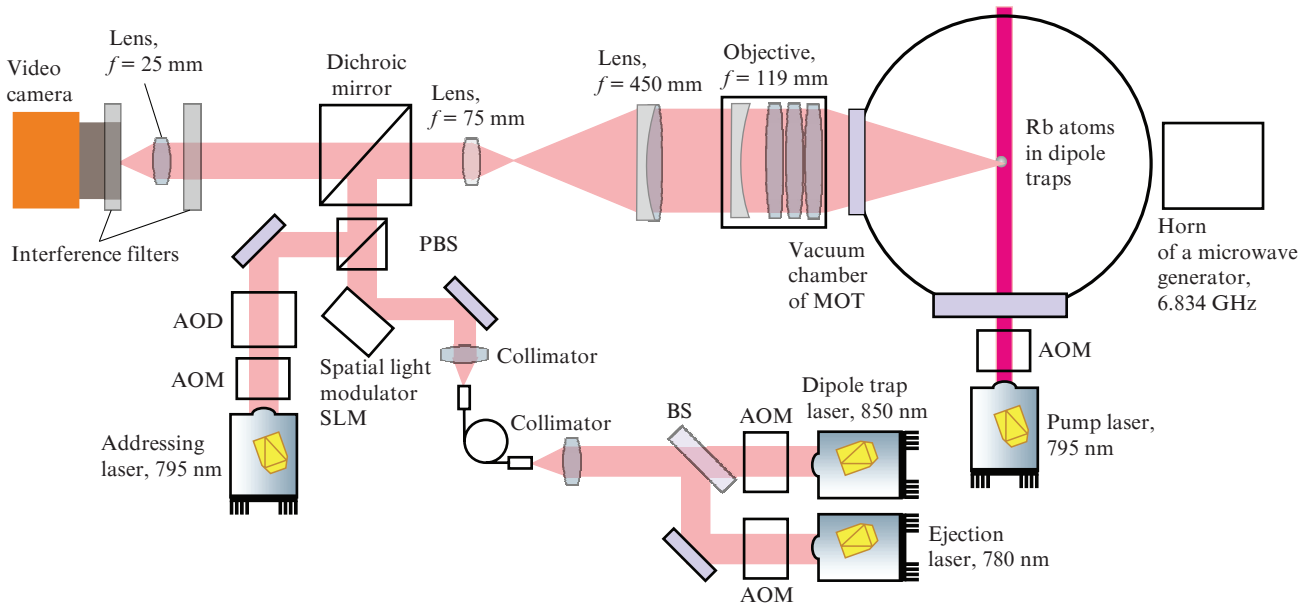

Figure 1. Schematic of an experimental setup for trapping two single ^{87}Rb atoms in two optical dipole traps, registering them, pumping them optically, and performing one-qubit quantum gates based on a microwave transition.

119 mm, pass through a telescope, a dichroic mirror, and are focused by a lens with $f = 25$ mm onto a FLIR Tau CNV digital sCMOS video camera. To increase the rate of collecting signals from single atoms, their images are projected onto single pixels of the video camera, the signals from which are then processed separately. To eliminate the influence of parasitic illumination at the dipole trap laser wavelength, two interference filters are installed in front of the video camera, transmitting radiation only at a wavelength of 780 nm. The image from the video camera is transferred to the computer via the CameraLink interface.

Demonstration of one-qubit quantum gates is carried out based on the magnetic dipole microwave transition $5S_{1/2}(F = 2, m_F = 0) \rightarrow 5S_{1/2}(F = 1, m_F = 0)$ at a frequency of 6.834 GHz between the hyperfine sublevels of the ground state, which serve as the working levels of qubits. In the diagram shown in Fig. 1, a pump laser is used for preliminary pumping of atoms to the Zeeman sublevel $5S_{1/2}(F = 2, m_F = 0)$ (initialisation of qubits), and the microwave generator induces Rabi oscillations between two working levels of qubits (rotation of the qubit state vector through a given angle). The pump beam tuned to resonance with the $5S_{1/2}(F = 2) \rightarrow 5P_{3/2}(F = 2)$ transition is launched orthogonally to the dipole trap beam, and its linear polarisation is directed along a uniform magnetic field of 4–5 Gs. The field is turned on by additional coils to lift the degeneracy of magnetic sublevels in atoms and to set the quantisation axis (in this case, the gradient magnetic field of the MOT is first turned off). Microwave radiation from the generator is fed through a window of the MOT vacuum chamber from the output of a homemade horn antenna based on a coaxial-waveguide junction. The horn is oriented in such a way that the magnetic component of the microwave field in the region of the atoms coincides in direction with the constant magnetic field, which ensures the maximum Rabi frequency.

The timing diagram of the experiment on the implementation of one-qubit quantum gates in two adjacent optical dipole traps is shown in Fig. 2. The experiment is carried out in a pulsed regime. Rubidium atoms are initially loaded into the MOT for 0.1–5 s and are simultaneously loaded into two optical dipole traps. The laser radiation of the dipole trap is modulated by rectangular pulses with a frequency of 1 MHz and a duty cycle of 1.25 in order to avoid the influence of light shifts on registration, pumping, and ejection of atoms in the absence of trap laser radiation (the light shift increases the detuning of optical transitions by tens of megahertz and decreases the fluorescence signal by several times), and keep the atoms in the trap during the pulses. The digital sCMOS video camera FLIR Tau CNV registers atoms as a sequence of images with an exposure time of 100–150 ms until the moment of loading single atoms into both traps and the appearance of the first signal of resonance fluorescence from both atoms. The trapping of two Rb atoms in two focused laser beams is monitored by the resonance fluorescence signal and the acquisition of an image of two atoms in traps on the video camera.

Upon loading single atoms into both traps, the procedure for implementing one-qubit quantum gates and measurements is launched. The cooling laser and the MOT gradient magnetic field are turned off. Then the beams of the cooling

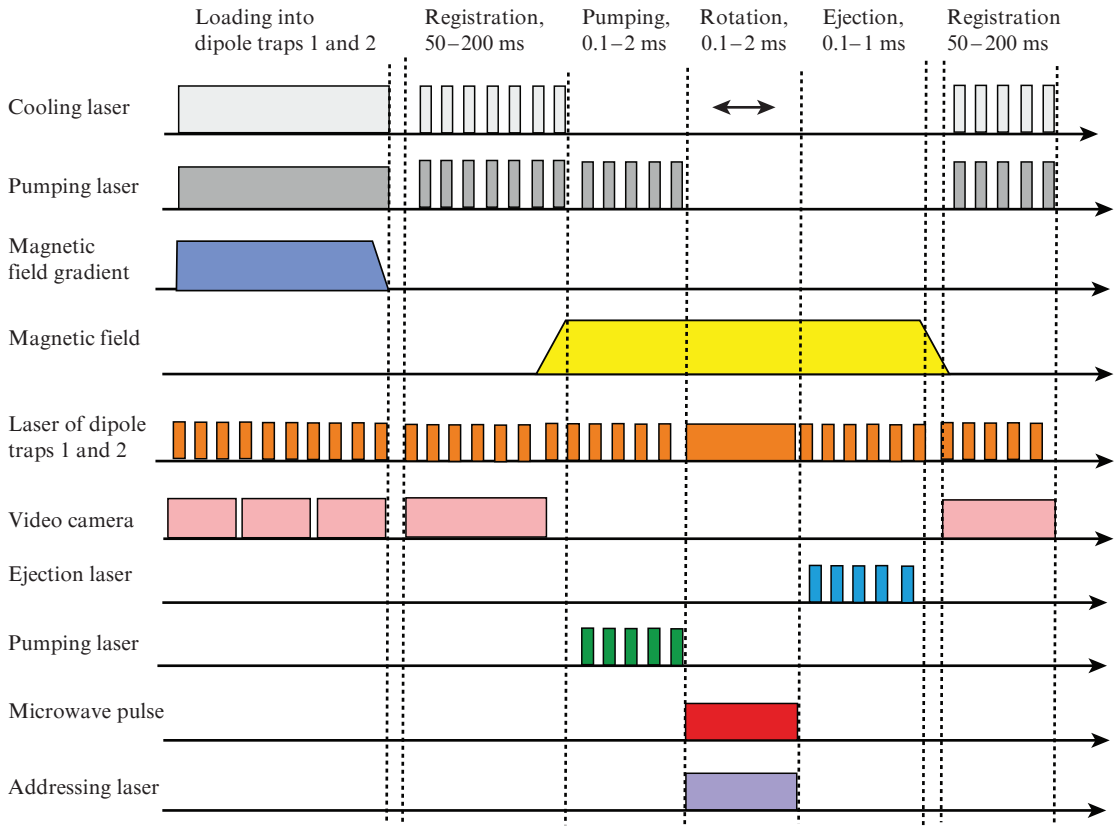

Figure 2. Time diagram of an experiment on the trapping of two single ^{87}Rb atoms, optical pumping, and implementation of one-qubit quantum gates based on a microwave transition with individual addressing in two traps.

laser and a video camera are turned on for the first registration of fluorescence signals from two trapped atoms. After that, the cooling laser is switched off and a uniform magnetic field is switched on. Then, a pump laser is switched on with radiation linearly polarised along the magnetic field, which acts on the atoms for 0.1–2 ms and pumps them to the Zeeman sublevel $5S_{1/2}(F = 2, m_F = 0)$ in the presence of repump laser radiation. Then the pump and repump lasers are turned off, and a microwave pulse is turned on to perform one-qubit quantum gates. The frequency of microwave radiation is tuned near the frequency of 6.834682 GHz of the $5S_{1/2}(F = 2, m_F = 0) \rightarrow 5S_{1/2}(F = 1, m_F = 0)$ clock transition between two working levels of a qubit, which are insensitive to an applied constant magnetic field.

To suppress Rabi oscillations in one of the atoms, an addressing laser pulse is switched on together with the microwave pulse. The optical frequency of the addressing laser beam can be varied to obtain a red or blue detuning of 20–100 GHz from the transitions of the D_1 absorption line in the ^{87}Rb atom. With such detunings, the excited state $5P_{1/2}$ is not populated, but the resonant frequency of the clock transition acquires a significant differential light shift (according to calculations, –5.7 kHz W^{-1} for the addressing laser radiation focused into a 10 μm diameter and with a detuning of +50 GHz), which exceeds typical width of microwave resonance (1–10 kHz) and is used to remove the addressed atom from resonance with microwave radiation when performing single-qubit gates. Since the addressing beam is focused only on one of the atoms, the microwave transition and Rabi oscillations will be suppressed in it, but they will be excited in the neighbouring atom. The addressing laser beam is tuned to one or the other qubit by changing the AOD frequency, and Rabi oscillations are recorded in both traps. To measure crosstalk in individual addressing, the degree of suppression of Rabi oscillations in each trap in the presence of the addressing laser radiation is determined.

Then the ejection laser is switched on to determine the final states of two atoms in neighbouring traps. For the ^{87}Rb isotope, the $5S_{1/2}(F = 2)$ state will correspond to the absence of a signal, since the ejection laser is tuned to the closed transition $5S_{1/2}(F = 2) \rightarrow 5P_{3/2}(F = 3)$ and expels atoms in the $5S_{1/2}(F = 2)$ state from the trap. The state $5S_{1/2}(F = 1)$ will correspond to the maximum signal, because the ejection laser does not affect atoms in this state. The final measurement of the quantum states of two atoms is carried out by turning on the cooling lasers again and recording the fluorescence signal on a digital video camera.

In the entire measurement procedure, the radiation from the cooling, pumping, repumping, and ejection lasers is modulated at a frequency of 1 MHz in antiphase with the modulation of the dipole trap laser radiation. This allows a significant reduction of the influence of parasitic processes in the switched-on trap, especially during the ejection process.

3. Trapping two ^{87}Rb atoms in two optical dipole traps

To implement two optical dipole traps, a special SLM phase mask was formed based on the modified Gerchberg–Saxton method [22] according to the methodology of our paper [12] (a similar technique is also used at the Moscow State University to create high-dimension arrays of single atoms [5]). The obtained profile of the radiation intensity distribution in the focus of the objective was previously measured using an intensity distribution meter DataRay Beam'R2. The diameter of each of the beams at the e^{-2} level did not exceed 9 μm, and the distance between the foci, at which the different beams were well resolved, was 12 μm. In this case, one could expect that Rb atoms in an optical dipole trap should be localised in a region with a smaller diameter, which would provide a better spatial resolution.

Then, atoms were trapped in two optical dipole traps according to the scheme shown in Fig. 1. Images of single atoms in two traps were projected onto separate pixels of a video camera. The average level of noise and background illumination was subtracted from the video signals of these pixels; therefore, the measured signal was proportional to the intensity of the resonant fluorescence of a single atom. After optimising all parameters (adjustment of the optical system, the power and detuning of laser radiation, the current of the Rb atom dispenser, and the exposure time of the video camera), an image of two single ^{87}Rb atoms in two adjacent optical dipole traps with a variable distance R between the centres of the traps was obtained (Fig. 3). The variation in R was achieved by changing the period of the SLM phase mask. At $R = 9$ μm, the images of two atoms partially overlapped (Fig. 3a), and at $R = 17$ μm, the images were well resolved (Fig. 3b). The observed size of the images of Rb atoms in individual traps was determined by the pixel size of the video camera (6.5 μm).

Since at $R = 17$ μm the image of each trap could fit on single pixels of the video camera, it was possible to record separately the signals of resonant fluorescence from each atom. The time dependence of the video signals had the character of chaotic pulses with a duration of 1–50 s, corresponding to the presence or absence of a single atom in each trap. This is the so-called telegraph signal, which has a pulsed character against the background of the video camera noise. In the experiments for both traps, independent telegraph signals were first obtained (Fig. 4a), which allowed measuring the average retention time of each atom in its own trap $\tau_1 = 16.6 \pm 2$ s. The observation of such telegraph signals indicated that the loading of strictly single atoms into each of the traps was achieved in the collisional blockade regime. Then, by analysing the correlations of two telegraph signals in time, the average time of the simultaneous confinement of two atoms in two traps was determined: $\tau_2 = 10.4 \pm 1$ s (Fig. 4b). This time is long enough to perform precise one- and two-qubit quantum gates with atoms in two traps.

4. Microwave transitions in two ^{87}Rb atoms with individual addressing

For individual addressing when performing one-qubit quantum gates, the focus of the addressing laser radiation was moved to one or the other trap by changing the frequency F_{AOD} of the AOD driver, which was verified in separate measurements in a model optical system. The addressing laser beam was manually adjusted along one of the coordinates, and along the other, it could be scanned using the AOD. At $F_{AOD} = 100.5$ MHz, the beam was exactly coincident with trap 1 (left trap in Fig. 3b), and at $F_{AOD} = 99.5$ MHz, with trap 2 (right trap in Fig. 3b).

Further experiments were performed on individual addressing of ^{87}Rb atoms in both traps to test the possibility of switching off the interaction with resonant microwave radiation. First, it was necessary to make sure that there was a light shift of microwave resonances when addressing each trap. When the addressing laser beam was strongly detuned

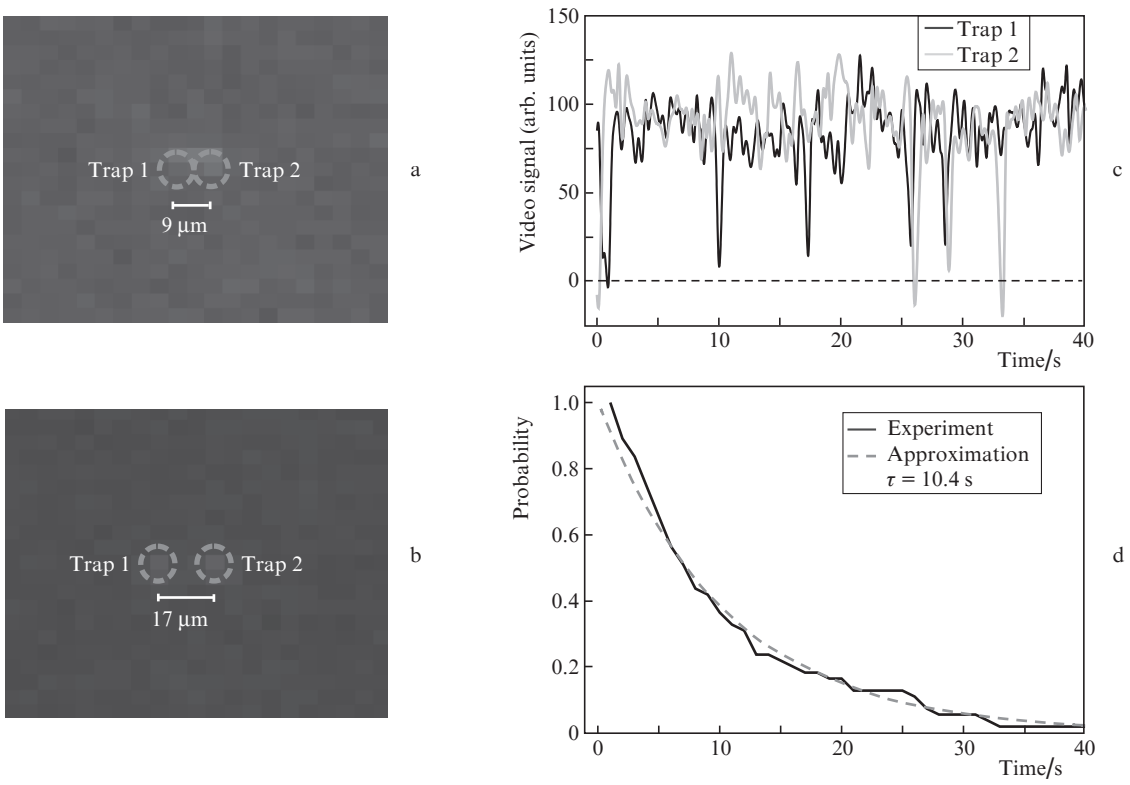

Figure 3. (a, b) Image of two single ^{87}Rb atoms in two adjacent optical dipole traps (light pixels, circled) with a distance between centres R = (a) 9 and (b) 17 μm; (c) telegraph signals of the fluorescence intensity of two single ^{87}Rb atoms in two neighbouring traps, and (d) time dependence of the probability of simultaneous trapping of two atoms in two traps determined from telegraph signals.

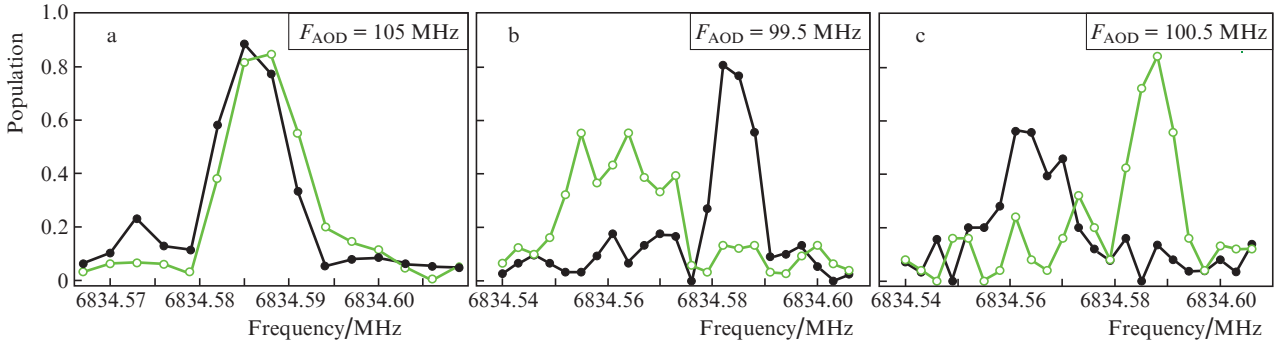

Figure 4. Experimental results on individual addressing of ^{87}Rb atoms in traps (●) 1 and (○) 2 upon interaction with resonant microwave radiation at F_{AOD} = (a) 105, (b) 99.5, and (c) 100.5 MHz.

(F_{AOD} = 105 MHz), microwave resonance was recorded in both traps (Fig. 4a) at a centre frequency of 6834.586 MHz {this frequency slightly differs from the reference value 6834.6826 MHz due to the error (~100 kHz) detected in setting the frequency of the used Agilent E8257D-567 microwave generator, as discussed in our paper [13]}. The resonance width of 10 kHz was mainly due to the Fourier spectrum width of the microwave pulse with a duration of 0.1 ms. When the focused addressing laser beam was tuned to trap 2 (F_{AOD} = 99.5 MHz), microwave resonance at a frequency of 6834.586 MHz was observed only in trap 1, and in trap 2 it was shifted by −21 kHz and broadened to 24 kHz by the addressing radiation (Fig. 4b). When the beam was tuned to trap 1 (F_{AOD} = 100.5 MHz), microwave resonance at a frequency of 6834.586 MHz was observed only in trap 2, and in trap 1 it was shifted by −22 kHz and broadened to 14 kHz by the addressing radiation (Fig. 4c). The widths and shapes of the shifted microwave resonances were somewhat different in traps 1 and 2. This indicates a certain difference in the parameters of the addressing radiation, which could be associated with insufficiently accurate coincidence of the addressing beam with each of the traps.

It can also be seen from Figs 4b and 4c that, with fine tuning to an unbiased microwave resonance with a frequency of 6834.586 MHz in one trap, the wing of a shifted resonance in another trap at this frequency has an amplitude of up to 12%–15%, which is actually a crosstalk upon individual addressing. To reduce it to 5%–10%, the radiation power of the addressing laser could be increased by several times.

Then, an experiment was carried out to observe Rabi oscillations upon individual addressing of ^{87}Rb atoms in two traps when interacting with resonant microwave radiation tuned to the centre of the clock transition at a frequency of 6834.586 MHz. The dots in Fig. 5 show the experimentally obtained Rabi oscillations. Each point corresponds to averaging the measured signal over 50 realisations. When the focused addressing laser beam was tuned to trap 2 (F_{AOD} = 99.5 MHz), Rabi oscillations were observed only in trap 1, and in trap 2 they were suppressed (Fig. 5a). When the beam was tuned to trap 1 (F_{AOD} = 100.5 MHz), Rabi oscillations were observed only in trap 2, and in trap 1 they were suppressed (Fig. 5b). The amplitude of the first Rabi oscillation reached 97%–98%, and crosstalk of individual addressing was less than 8% in trap 2 (Fig. 5a) and less than 5% in trap 1 (Fig. 5b).

As noted in our paper [13], the clock microwave transition in the ^{87}Rb atom under ideal conditions (without parasitic processes) is an ideal two-level system without relaxation of populations and phases. In such a system, Rabi oscillations do not decay. However, in practice, there are always parasitic processes (fluctuations in the frequency and power of the microwave generator, magnetic field noise, transitions induced by background thermal radiation, fluctuations in the exact resonance frequency due to light shifts induced by the dipole trap laser), which lead to damping of Rabi oscillations and stabilisation of the populations at some stationary values. In this case, the time evolution of the populations in the two-level system is described by a more complex expression. In Ref. [13], we used a formula from our paper [23], obtained by solving equations for the density matrix in the presence of relaxation of populations and phases. However, it seems more adequate to use another formula that we obtained analytically in Ref. [24], where only the relaxation of phases with a rate Γ is taken into account, but there is no population relaxation in the two-level system. In Ref. [24], it was derived for the evolution of populations in the dipole-dipole interaction of Rydberg atoms, but after redefining the variables, it is applicable to our case as well. For the probability of a microwave transition in a two-level system with phase relaxation, this formula reads

$$\rho(t) \approx \frac{1}{2} - \frac{\delta^2/2}{\Omega^2+\delta^2}\exp\left(-\frac{\Omega^2}{\Omega^2+\delta^2}\Gamma t\right) - \frac{\Omega^2/2}{\Omega^2+\delta^2}\exp\left(-\frac{\Omega^2/2+\delta^2}{\Omega^2+\delta^2}\Gamma t\right)\cos\left(\sqrt{\Omega^2+\delta^2}\,t\right). \quad (1)$$

Here Ω is the Rabi frequency of the magnetic dipole clock transition, and δ is the detuning from the exact clock transition frequency, taking into account the possible light frequency shift under the action of the dipole trap laser, if the measurement is carried out with the trap turned on. Formula (1) is valid at $\Omega > 3\Gamma$, i.e., at a sufficiently slow phase relaxation. It also describes the spectrum of the transition when scanning δ, the interaction time t_0 being fixed.

In exact resonance (δ = 0), the population oscillates between the initial and final states at the frequency Ω (Rabi oscillations):

$$\rho(t) \approx \frac{1}{2}\left[1 - \exp\left(-\frac{\Gamma t}{2}\right)\cos(\Omega t)\right]. \quad (2)$$

In the absence of phase relaxation (Γ = 0), Rabi oscillations last infinitely long. For $\Gamma \neq 0$, the coherence (decay) time of Rabi oscillations can be defined as $\tau = 2/\Gamma$ and measured by making a comparison between experiment and Eqn (2). At $t \to \infty$, the population reaches the stationary value 1/2.

Solid curves in Fig. 5 show the results of the approximation of experimental points in both traps using Eqns (1) and (2). For non-addressed traps with complete Rabi oscillations, we took Eqn (2), from which we obtained the values $\Omega/2\pi$ = 5.0 ± 0.05 kHz and τ = 4.0 ± 0.5 ms for trap 1 (Fig. 5a) and $\Omega/2\pi$ = 5.1 ± 0.05 kHz and τ = 4.0 ± 0.5 ms for trap 2 (Fig. 5b).

For addressed traps with suppressed Rabi oscillations, we took Eqn (1) with large detunings δ and values of Ω measured above. Approximate values $\delta/2\pi$ = 20 ± 5 kHz and τ = 0.4 ± 0.2 ms for trap 2 (Fig. 5a) and for trap 1 (Fig. 5b) were obtained from it. These values have greater uncertainty due to the large effective Rabi frequency $\sqrt{\Omega^2+\delta^2}$ at larger δ and shorter coherence time due to additional broadening and non-Lorentzian microwave resonance contour in addressed traps, as can be seen from Fig. 4. Nevertheless, this approximation satisfactorily describes the slow rise of the average signal level in these traps over time to estimate crosstalk upon individual addressing.

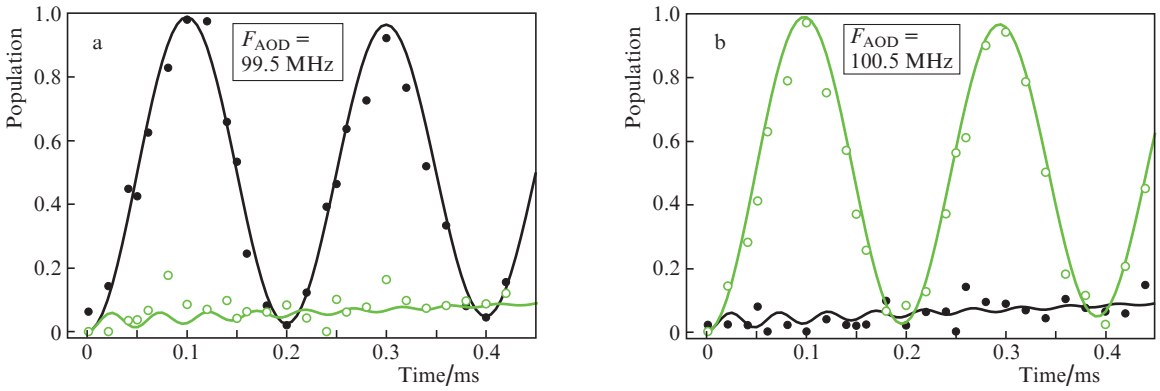

Figure 5. Rabi oscillations upon individual addressing of ^{87}Rb atoms in traps (•) 1 and (○) 2 upon interaction with resonant microwave radiation tuned to the centre of the clock transition at a frequency of 6834.586 MHz at F_{AOD} = (a) 99.5 and (b) 100.5 MHz.

5. One-qubit quantum gates on microwave transitions in two ^{87}Rb atoms with individual addressing

The presence of individually addressed Rabi oscillations in Fig. 5 actually corresponds to the demonstration of individually addressed one-qubit quantum gates from different initial states of qubits in two neighbouring traps. The determination of the fidelity of performing one-qubit quantum gates in each trap is performed by experimental measurement of the transition probabilities for Rabi oscillations and constructing truth tables, when the qubit state vector rotates through an angle π for the NOT gate and an angle π/2 for the analogue of the Hadamard gate H for various initial states (logical '0' and '1'). The initial state $5S_{1/2}(F = 2, m_F = 0)$ is selected as the logical '0', and the final state $5S_{1/2}(F = 1, m_F = 0)$ is selected as the logical '1'. To prepare the initial state '1', the NOT gate is first used, which is combined with the subsequent rotation of the qubit. The completion of each one-qubit gate corresponds to pre-defined areas of the microwave pulses.

Figure 6 shows an experimental record of the Rabi oscillations from Fig. 5, reduced to the scale of the microwave pulse area according to the measured Rabi frequencies in two traps. Vertical lines set points 1–4 for the intersection of areas π/2, π, 3π/2, and 2π with experimental oscillations to determine the fidelity of performing single-qubit gates.

In the case of the initial state '0', the Hadamard gate corresponds to a rotation through an angle π/2, while the microwave pulse ends at time 1 (pulse with area π/2). After rotation through an angle π/2, the population at point 1 in Fig. 6a for trap 1 is 0.43 ± 0.02 instead of the ideal value of 0.5. Thus, the fidelity of the Hadamard gate from the initial state '0' in trap 1 is 86% ± 4%. In this case, the amplitude of the cross-signal in trap 2 is 0.037 ± 0.01, which corresponds to an individual addressing error of 3.7% ± 1%. A similar analysis of Rabi oscillations in trap 2 (Fig. 6b) gives the population at point 1, equal to 0.41 ± 0.02, and the fidelity of the Hadamard gate from the initial state '0' in trap 2, equal to 82% ± 4%. In this case, the amplitude of the cross-signal in trap 1 is 0.078 ± 0.01, which corresponds to an individual addressing error of 7.8% ± 1%.

In the case of the initial state '0', the NOT gate corresponds to a rotation through the angle π, the microwave pulse ends at time 2 (pulse with area π). In Fig. 6a, after rotation through an angle π, the population at point 2 for trap 1 is 0.98 ± 0.02 instead of the ideal value 1, i.e. the fidelity of the NOT gate from the initial state '0' in trap 1 is 98% ± 2%. In this case, the amplitude of the cross-signal in trap 2 is 0.085 ± 0.01, which corresponds to an individual addressing error of 8.5% ± 1%. For trap 2 (Fig. 6b), the population at point 2 is 0.97 ± 0.02, and the fidelity of the NOT gate from the initial state '0' is 97% ± 2%, while the amplitude of the cross-signal in trap 1 is 0.01 ± 0.01 (error of individual addressing 1% ± 1%).

To construct truth tables corresponding to the initial state '1', this state is preliminarily prepared by rotating the qubit through an angle π (point 2 in Fig. 6).

To execute the Hadamard gate from state '1', an additional rotation through the angle π/2 occurs, which corresponds to the end of the microwave pulse at time 3. In Fig. 6, and after rotation from point 2 through angle π/2, the population at point 3 for trap 1 is 0.53 ± 0.02 instead of the ideal value of 0.5 (the fidelity of the Hadamard gate from the initial state '1' in trap 1 is 94% ± 4%). The cross-signal amplitude in trap 2 is 0.042 ± 0.01, corresponding to an individual addressing error of 4.2% ± 1%. For trap 2 (Fig. 6,b), the population at point 3 is 0.44 ± 0.02, and the fidelity of the Hadamard gate from the initial state '0' in trap 2 is 88% ± 4%. The amplitude of the cross-signal in trap 1 is 0.018 ± 0.01 (individual addressing error 1.8% ± 1%).

To execute the NOT gate from state '1', an additional rotation through an angle π occurs, the microwave pulse ends at time 4. In Fig. 6, and after rotation from point 2 through an angle π, the population at point 4 for trap 1 is 0.02 ± 0.02 instead of the ideal value of 0, then the fidelity of the NOT gate from the initial state '1' for trap 1 is 98% ± 2%. In trap 2, the cross-signal amplitude is 0.083 ± 0.01 (individual addressing error 8.3% ± 1%). For trap 2 (Fig. 6b), the population at point 4 is 0.078 ± 0.02, and the fidelity of the NOT gate from the initial state '1' in trap 2 is 92% ± 2%. In trap 1, the cross-signal amplitude is 0.02 ± 0.01 (individual addressing error 2% ± 1%).

Based on the results of these direct measurements, a truth table was compiled for each of the one-qubit gates and cross-talk in each of the two traps (Table 1). It can be seen from the table that the Hadamard gates have the greatest implementation error, and the NOT gates achieve much higher fidelity. This is due to the fact that for NOT gates in Fig. 6 the dependence of the signal on the area of the microwave pulse around points 2 and 4 is quadratic, and for Hadamard gates around points 1 and 3 it is linear. As already mentioned, each experimental point in Fig. 6 corresponds to the averaging of the

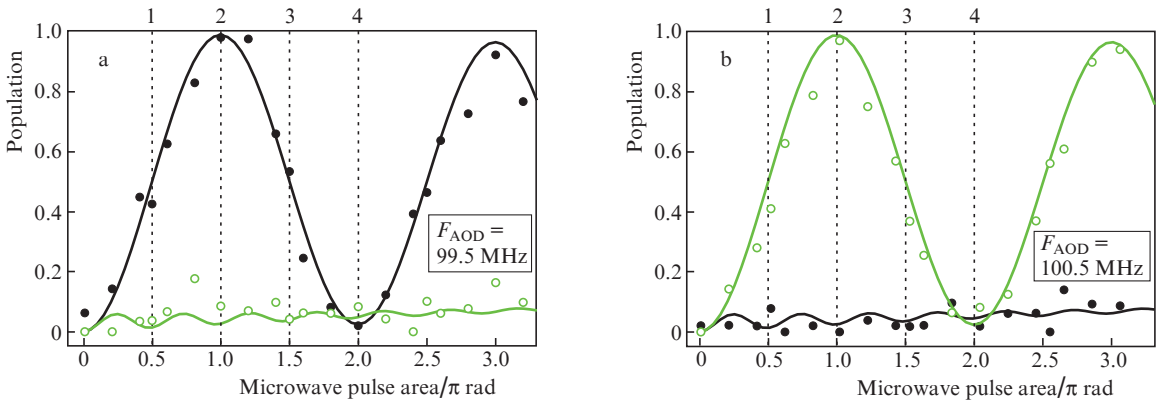

Figure 6. Experimental records of Rabi oscillations corresponding to Fig. 5, reduced to the scale of the microwave pulse area according to the measured Rabi frequencies in traps (●) 1 and (○) 2 at F_{AOD} = (a) 99.5 and (b) 100.5 MHz.

Table 1. Truth table for the fidelity of one-qubit gates and crosstalk in each of the two traps from direct measurements with different initial states of qubits.

Initial state of a qubit	Fidelity of H gate	Addressing error uring H gate	Fidelity of NOT gate	Addressing error during NOT gate
0	Trap 1 86% ± 4%	Trap 2 3.7% ± 1%	Trap 1 98% ± 2%	Trap 2 8.5% ± 1%
	Trap 2 82% ± 4%	Trap 1 7.8% ± 1%	Trap 2 97% ± 2%	Trap 1 1% ± 1%
1	Trap 1 94% ± 4%	Trap 2 4.2% ± 1%	Trap 1 98% ± 2%	Trap 2 8.3% ± 1%
	Trap 2 88% ± 4%	Trap 1 1.8% ± 1%	Trap 2 92% ± 2%	Trap 1 2% ± 1%

measured signal over 50 realisations, and so the recording of each point takes from one to several minutes. If during such a long recording there is a drift in the intensity of the dipole traps or the frequency of the microwave generator, this leads to much larger signal errors at points 1 and 3, which are in a linear section, than at points 2 and 4, which are actually in saturation and are less sensitive to drifts.

6. Conclusions

From Table 1, it can be found that in our experiment the average fidelity of performing one-qubit quantum gates with two individually addressed Rb atoms in two adjacent traps was 92% ± 3%, and the level of crosstalk was 4.7% ± 1%. However, in the literature on quantum computing, it is generally accepted to present the results of measuring the fidelity of quantum gates, renormalised taking into account the errors in preparing the initial state and measuring the final state of qubits, the so-called state-preparation-and-measurement (SPAM) errors. This is because the fidelity F of performing quantum gates in the course of the entire quantum computing algorithm will be determined only by the error in the rotation of the qubit state vector through specified angles and will not depend on the SPAM error.

One of the methods for separating F from SPAM error based on the results of direct measurements is randomized benchmarking (RB) [25], in which a sequence of a set of randomly selected one-qubit quantum gates with a known total area of rotating pulses is performed. In the absence of a rotation error, such a sequence should give a strictly defined final state of the qubit, and in the presence of a rotation error, it will have some error. Experiments should measure the dependence of the probability of the desired final state of the qubit on the number of rotations. In this case, the SPAM error will only affect the measurement fidelity after the first rotation, and the value of F is extracted from the slope of the obtained dependence on the number of rotations and does not depend on SPAM error.

For example, in experimental studies [9, 10], such measurements were carried out with qubits based on single Cs or Rb atoms in arrays of optical dipole traps when performing one-qubit quantum gates on microwave transitions, as in our experiment. In these studies, the fidelity of obtaining a given state after the first rotation was about 99%, and after performing subsequent rotations, a much smaller average value of the error of an individual rotation $F < 10^{-3}–10^{-4}$ was determined. In fact, the first rotation error was completely determined by the SPAM error.

Thus, the values of the accuracies presented in Table 1 based on the results of direct measurements should be renormalised to SPAM errors to determine the true average value of the rotation error F (averaging is carried out over all quantum gates from both initial states). Since the experimental implementation of the RB method would require a large amount of additional work, here we restrict ourselves to estimating the magnitude of the SPAM errors in our experiments. It is at the level of 5% and is the sum of the error of optical pumping (2%–3%) measured earlier in [13], the loss of atoms from the trap during the cycle (1%–2%), and the parasitic transfer of populations when determining the states of atoms by the method of ejection (2%–3%). Then the obtained average fidelity of one-qubit gates of 92% ± 3% should be divided by 0.95 for a rough estimate. As a result, we obtain an estimate of the true average value of the error of rotations F = 97% ± 3%. This fidelity of performing one-qubit quantum gates with individual addressing is high enough for setting up experiments on the implementation of two-qubit quantum gates based on short-term excitation of atoms to Rydberg states.

Acknowledgements. The authors are grateful to M. Saffman and S.S. Straupe for useful discussions. This work was supported by the Russian Foundation for Basic Research (in part of the theory of quantum informatics, Grant No. 19-52-15010), the Russian Science Foundation (in part of the experimental implementation of quantum gates, Grant No. 18-12-00313), the Advanced Research Foundation (in part of developing laser excitation systems and pumping atoms in a dipole trap), and Novosibirsk State University (in part of developing a laser cooling system in a magneto-optical trap).

References

1. Saffman M., Walker T.G., Mølmer K. *Rev. Mod. Phys.*, **82**, 2313 (2010).
2. Ryabtsev I.I., Beterov I.I., Tretyakov D.B., Entin V.M., Yakshina E.A. *Phys. Usp.*, **59**, 196 (2016) [*Usp. Fiz. Nauk*, **182**, 206 (2016)].
3. Saffman M. *J. Phys. B*, **49**, 202001 (2016).
4. Graham T.M., Kwon M., Grinkemeyer B., Marra Z., Jiang X., Lichtman M.T., Sun Y., Ebert M., Saffman M. *Phys. Rev. Lett.*, **123**, 230501 (2019).
5. Samoylenko S.R., Lisitsin A.V., Schepanovich D., Bobrov I.B., Straupe S.S., Kulik S.P. *Las. Phys. Lett.*, **17** (2), 025203 (2020).
6. Yavuz D.D., Kulatunga P.B., Urban E., Johnson T.A., Proite N., Henage T., Walker T.G., Saffman M. *Phys. Rev. Lett.*, **96**, 063001 (2006).
7. Jones M.P.A., Beugnon J., Gaëtan A., Zhang J., Messin G., Browaeys A., Grangier P. *Phys. Rev. A*, **75**, 040301 (2007).
8. Weitenberg C., Endres M., Sherson J.F., Cheneau M., Schauß P., Fukuhara T., Bloch I., Kuhr S. *Nature*, **471**, 319 (2011).

9. Xia T., Lichtman M., Maller K., Carr A.W., Piotrowicz M.J., Isenhower L., Saffman M. *Phys. Rev. Lett*., **114**, 100503 (2015).
10. Sheng C., He X., Xu P., Guo R., Wang K., Xiong Z., Liu M., Wang J., Zhan M. *Phys. Rev. Lett*., **121**, 240501 (2018).
11. Beterov I.I., Yakshina E.A., Tretyakov D.B., Entin V.M., Singh U., Kudlaev Ya.V., Mityanin K.Yu., Panov K.A., Al'yanova N.V., Ryabtsev I.I. *Quantum Electron*., **50** (6), 543 (2020) [*Kvantovaya Elektron*., **50** (6), 543 (2020)].
12. Ryabtsev I.I., Mityanin K.Yu., Beterov I.I., Tretyakov D.B., Entin V.M., Yakshina Ye.A., Al'yanova N.V., Neizvestnyi I.G. *Optoelectron. Instrument. Proc*., **56** (5), 510 (2020) [*Avtometriya*, **56** (5), 72 (2020)].
13. Beterov I.I., Yakshina E.A., Tretyakov D.B., Entin V.M., Alyanova N.V., Mityanin K.Yu., Ryabtsev I.I. *J. Exp. Theor. Phys*., **132** (3), 341 (2021) [*Zh. Eksp. Teor. Fiz*., **159** (3), 409 (2021)].
14. Sautenkov V.A., Saakyan S.A., Bobrov A.A., Kudrinskiy D.A., Vilshanskaya E.V., Zelener B.B. *J. Russ. Laser Res*., **40**, 230 (2019).
15. Davletov E.T., Tsyganok V.V., Khlebnikov V.A., Pershin D.A., Shaykin D.V., Akimov A.V. *Phys. Rev. A*, **102**, 011302(R) (2020).
16. Fedorova E.S., Tregubov D.O., Golovizin A.A., Mishin D.A., Provorchenko D.I., Khabarova K.Yu., Sorokin V.N., Kolachevsky N.N. *Quantum Electron*., **50** (3), 220 (2020) [*Kvantovaya Elektron*., **50** (3), 220 (2020)].
17. Vinogradov V.A., Karpov K.A., Lukashov S.S., Turlapov A.V. *Quantum Electron*., **50** (6), 520 (2020) [*Kvantovaya Elektron*., **50** (6), 520 (2020)].
18. Mashko A.M., Meisterson A.A., Afanasyev A.E., Balykin V.I. *Quantum Electron*., **50** (6), 530 (2020) [*Kvantovaya Elektron*., **50** (6), 530 (2020)].
19. Barredo D., de Léséleuc S., Lienhard V., Lahaye T., Browaeys A. *Science*, **354**, 1021 (2016).
20. Pritchard J.D., Isaacs J.A., Saffman M. *Rev. Sci. Instrum*., **87**, 073107 (2016).
21. Schlosser N., Reymond G., Grangier P. *Phys. Rev. Lett*., **89**, 023005 (2002).
22. Gerchberg R.W., Saxton W.O. *Optic (Stuttgart)*, **34**, 237 (1972).
23. Entin V.M., Yakshina E.A., Tretyakov D.B., Beterov I.I., Ryabtsev I.I. *J. Exp. Theor. Phys*., **116**, 721 (2013) [*Zh. Eksp. Teor. Fiz*., **143** (5), 831 (2013)].
24. Yakshina E.A., Tretyakov D.B., Beterov I.I., Entin V.M., Andreeva C., Cinins A., Markovski A., Iftikhar Z., Ekers A., Ryabtsev I.I. *Phys. Rev. A*, **94**, 043417 (2016).
25. Knill E., Leibfried D., Reichle R., Britton J., Blakestad R.B., Jost J.D., Langer C., Ozeri R., Seidelin S., Wineland D.J. *Phys. Rev. A*, **77**, 012307 (2008).